The Impact Response of Cranial Bone

J. A. Motherway[1] and M. D. Gilchrist[1, 2]
[1] School of Mechanical Engineering, University College Dublin; [2] School of Human Kinetics, University of Ottawa, Canada.

ABSTRACT

Linear and depressed skull fractures are frequent mechanisms of head injury and are often associated with traumatic brain injury. Accurate knowledge and understanding of the fracture of cranial bone can provide insight into the prevention of skull fracture injuries and associated lesions of soft neural tissue and help aid the design of energy absorbing head protection systems. Cranial bone is a complex material comprising of a three-layered structure: external layers consisting of compact, high-density cortical bone and a central layer consisting of a low-density, irregularly porous structure. In the current study, a significantly large set of cranial bone specimens (parietal and frontal bones) were extracted from 8 crania and, after μCT imaging, the specimens were tested in a three-point bend set-up at dynamic speeds. Important mechanical and morphological properties were calculated for each specimen. The mechanical properties were consistent with those previously reported in the literature. Potential correlations between the calculated parameters were examined statistically. Testing speed, strain rate, cranial sampling position and intercranial variation were found to have a significant effect on some or all of the computed mechanical parameters. In addition, structurally detailed 3D finite element (FE) models were developed from the μCT data and validation and verification of these models is in progress with a view to improving the skull material and failure definitions in the UCD 3D-FE model of the skull-brain complex, currently used to aid helmet design.

INTRODUCTION

Human cranial bone has previously been tested in compression, tension and bending (Evans and Lissner, 1957; McElhaney et al., 1970; Wood, 1971; Hubbard, 1971; McPherson and Kriewall, 1980; Margulies and Thibault, 2000; Delille et al., 2003 and Delille et al., 2007; Coats and Margulies, 2006). The majority of these studies concentrate on fetal cranial bone at quasi-static testing speeds. However, fetal and adult cranial bones are vastly different materials. Fetal cranial bone is a thin, non-homogeneous cortical bone layer with a highly directional fibre orientation (McPherson and Kriewall, 1980). Mature adult cranial bone has stiff outer cortical strata and an inner energy absorbing porous lightweight core, the diploë. Thus the elastic modulus of adult cranial bone is higher (Margulies and Thibault, 2000) and the diploë acts to increase its thickness thereby increasing its bending strength. Furthermore, the diploë is an efficient energy absorbing layer and stiffens the whole sandwich structure. The aim of this study is to characterise the response of adult cranial bone under dynamic impacts and to use those results to improve the skull material and failure definitions in the UCD 3D-FE model of the skull-brain complex.

METHODS

Specimen Preparation:

Adult cranial bones were obtained from 8 fresh-frozen (refrigeration at −20 °C) cadavers (F=4, M=4; 81±11 years old). 63 specimens (6 cm×1 cm) were obtained from the parietal and frontal bones using a vertical band saw and gently filing the cut faces to ensure accurate dimensions. The thickness and initial curvature of the specimens could not be controlled but care was taken to extract specimens with the least curvature and the orientation of specimens was kept as uniform as possible (Figure 1(A)).

All specimens were scanned using a μCT scanner (MTM Tomohawk System; resolution= 56.9 μm) with a solid calibration phantom. Before testing, each specimen was instrumented with support structures, made from rigid two-part epoxy resin, to eliminate slippage during testing and to give a flat surface on which to rest the specimens, in addition, this set-up still allowed specimen rotation in bending. The effective span length for the tests was 3 cm (the distance between the two supporting pins).

Mechanical Testing:

Dynamic three-point bend tests were carried out at three testing speeds (0.5, 1 and 2.5 m/s). The test set-up, (Figure 1(B)), consisted of a static upper fixture with two metal support pins (radius 4 mm) for holding the specimens. This was rigidly attached to a quartz load cell (Type 9331B, Kistler, Switzerland) for measuring the incident force. The impacting pin (radius 6 mm) was displacement controlled using a servo-hydraulic Instron 8502 testing bench. The displacement was measured during each test using a high accuracy laser displacement sensor (Type M5L/20, GEPA, Munich) attached to the Instron actuator head. A data acquisition system was used independently of the Instron and all data was sampled at 33 kHz. The force–displacement curve for each test was recorded and each test was also captured using high speed video (Phantom V5.1 monochrome camera, Photo-Sonics, England) at between 20,000 and 25,000 frames-per-second.

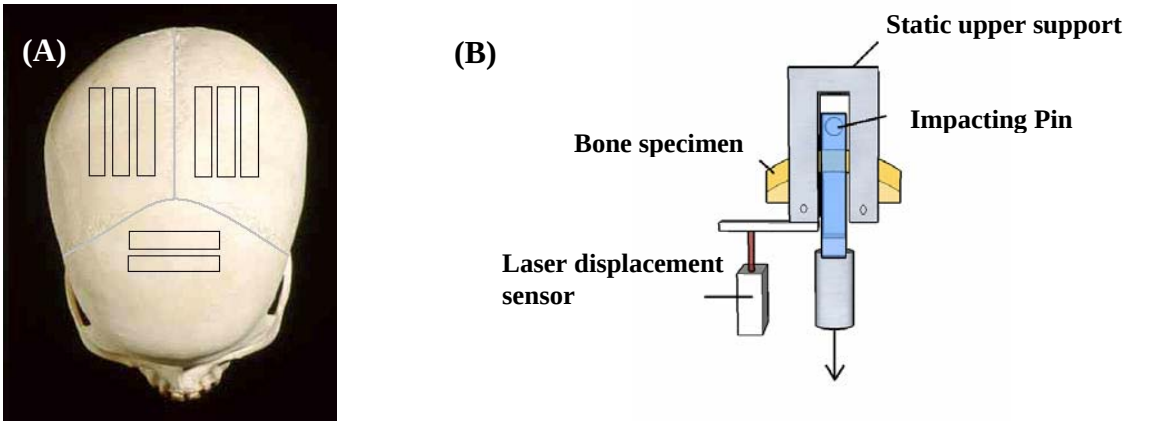

Figure 1: (A) The orientation of the specimens taken from each cranial vault, (B) A schematic of the three-point bending test set-up.

Data Analysis:

Three specimens were excluded from further analysis due to their lateral slippage during testing. For the remaining specimens, the following mechanical and morphological parameters were calculated (Further details can be found in Motherway et al. (2009)):

Elastic modulus (E): Timoshenko beam theory was used because, on average, the span length (L) to thickness ratio was less than 8:

$$(1)\ E = \frac{F\,L^3}{48\,I_{eq}} \cdot \frac{1}{\left(d_{total} - d_{shear}\right)} \qquad \text{where: } (2)\quad d_{shear} = \frac{F\,L}{4\,G\,A\,K}$$

The shear moduli (G) used were average adult values from Peterson and Dechow (2002, 2003) (parietal:6.8GPa; frontal:6.4GPa). The cross-section (assumed rectangular) required a shear correction factor (K) of 5/6 (Kaneko, 1975; Timoshenko et al., 1975; Caprino et al., 2009). I_{eq}= 2nd moment of inertia, d_{total}/d_{shear}= total/shear displacement, F= load at mid-span and A= cross-sectional area.

Energy absorbed to failure ($U_{failure}$): Calculated from the force–displacement curves and normalised by specimen volume (Margulies and Thibault, 2000):

$$(3)\ U_{failure} = \frac{\int F\,d\delta}{V}$$

$\int F\,d\delta$ = integral of force-displacement curve and V= volume of span length of specimen.

Maximum bending stress or rupture stress (σ_{rupt}): Calculated using simple beam theory (Timoshenko and Goodier, 1970; Margulies and Thibault, 2000). Cross-section assumed rectangular.

$$(4)\ \sigma_{rupt} = \frac{3P\left(\frac{L}{2}\right)}{4\,c^2} - 0.133\left(\frac{P}{c}\right)$$

P= maximum force per unit width of the specimen and c= half-depth of beam.

Morphological parameters: The percent bone volume and percent porosity of the cranial specimens were calculated from the μCT scans using CT Analyser (Version 1.6.1.1, Skyscan, Belgium). The average specimen thicknesses were calculated from the μCT scan sets using custom code written in Matlab 7.3.0 (The MathsWorks Inc.).

Statistical Analysis:

The general linear model statistical procedure and subsequent post-hoc multiple comparison test known as Tukey–Kramer were used to determine the effect of test parameters on the calculated mechanical data. This method was used as it can account for the unbalanced group sizes compared in this analysis. Correlations were measured using the Pearson coefficient and two-tailed p-values are reported. The significance level for all analyses was set as $p<0.05$ and all statistical analyses were performed using SAS 9.1 (SAS Institute Inc., USA).

Finite Element Modelling:

A rigorous plan for the finite element (FE) model generation and subsequent verification, validation and sensitivity analysis was drawn up according to best practice in the literature. FE meshes of the bone specimens were generated from their μCT scan set using the commercial software package Simpleware. These specimen meshes were then imported into ABAQUS 6.9, the model was implemented and run. A sensitivity analysis of the model boundary conditions has been completed and mesh convergence testing and sensitivity to material definitions is currently underway. A density correlation phantom was scanned with the bone specimens to allow the direct mapping of the bone material properties from the μCT scan's greyscale values.

RESULTS

Figure 2 shows a typical force-displacement curve measured from the three-point bending tests. These curves were used to calculate the mechanical properties summarised in Table 1.

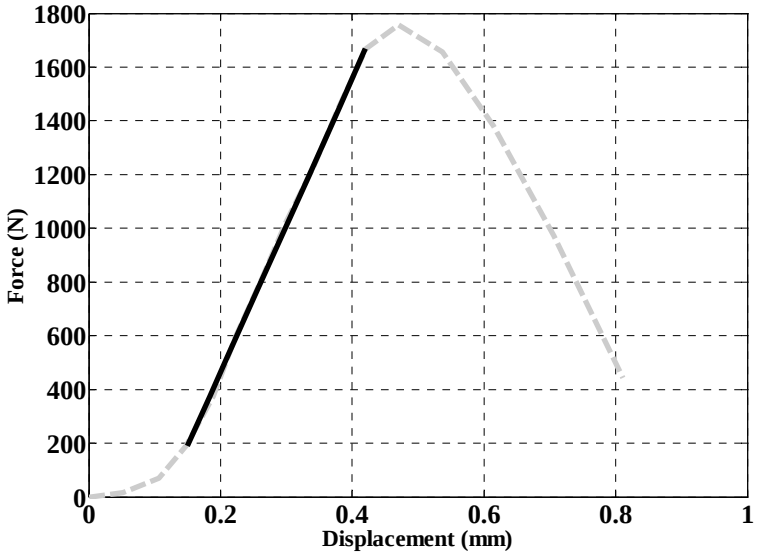

Figure 2: Measured force-displacement graph for a cranial specimen tested at 2.5m/s.

Table 1: Calculated mechanical properties of human cranial bone in three-point bending (Standard deviation in parentheses)

Speed (m/s)	N	Max Force (N)	E (GPa)	σ_{rupt} (MPa)	U_o (kN.m/m^3)	Strain Rate (s^{-1})
0.5	18	803.1 (345.3)	7.46 (5.39)	85.11 (23.55)	123.15 (56.77)	21.16 (6.79)
1	20	791.4 (387.4)	10.77 (9.38)	86.44 (27.08)	115.87 (72.97)	28.25 (7.82)
2.5	22	1221.1 (524.8)	15.54 (10.29)	127.84 (46.88)	167.82 (104.19)	107.20 (26.07)

Loading Rates: It was found that the maximum force to failure ($p=0.0007$), elastic modulus ($p=0.0243$) and maximum bending stress ($p=0.0012$) were significantly affected by the loading rates. According to the Tukey-Kramer post-hoc test, it was found that noticeably higher maximum forces were associated with the higher speed (2.5m/s) when compared to both of the lower speeds (0.5 and 1m/s). Similarly, the maximum bending stress was significantly larger at the highest speed (2.5m/s). In the case of the elastic modulus, a significant difference was only found between the lowest and the highest speeds (0.5m/s Vs 2.5m/s). A general trend to note is that the stiffness of cranial bone increases with average impact speed. Significant modest correlations were found between strain rate and maximum force to failure ($r^2=0.2861$; $p<0.0001$), maximum bending stress ($r^2=0.0844$; $p=0.0256$) and the energy absorbed until failure ($r^2=0.1063$; $p=0.0117$).

Cranial Position: The cranial sampling position (parietal or frontal) was found to significantly affect the resulting values only for the maximum force to failure ($p=0.0159$), the 2nd moment of inertia ($p=0.0117$) and the energy absorbed until failure ($p=0.0131$). On further examination, it was found that the frontal group required the highest average forces at failure and absorbed the most energy prior to failure. This may be partially explained by the fact that the frontal bone had a significantly higher average 2nd moment of inertia ($3.37e^{-10}\pm1.78e^{-10}m^4$) than the parietal bones ($2.48e^{-10}\pm1.78e^{-10}m^4$).

Intercranial Variation: The intercranial variation between the eight calvaria had a significant effect on all mechanical parameters: the moment of inertia ($p<0.0001$), elastic modulus ($p=0.0004$), maximum force at failure ($p<0.0001$), energy absorbed until failure ($p<0.0001$) and maximum bending stress ($p<0.0001$).

Morphological Parameters: The average percent porosity was 10.24±3.72% (frontal) and 13.94±4.02% (parietal) and the average percent bone volume was 74.94±7.17% (frontal) and 69.59±10.62% (parietal). A modest correlation was found between percent bone volume and both the elastic modulus ($r^2=0.1963$; $p=0.0004$) and the maximum bending stress ($r^2=0.2708$; $p<0.0001$). It was found that the average thickness for the frontal bones (6.89±1.43mm) was greater than that for the parietal bones (6.30±1.68mm).

Finite Element Modelling: A sensitivity study was done to determine the most appropriate boundary conditions for the models. It was found that it was possible to simplify the boundary conditions significantly to reduce computational cost without a significant cost in

terms of model accuracy. Further details in Appendix A. Mesh convergence testing and material definition sensitivity testing are ongoing.

CONCLUSIONS

The calculations of this study make some assumptions about the cranial bone specimens. While three-point bend tests allow for the use of simply shaped rectangular specimens, the associated Timoshenko beam theory makes assumptions about the material's structure: beams are assumed to be composed of homogeneous, isotropic material with a uniform cross-section along their length. Neither of these assumptions are perfect for the present cranial bone specimens. However, using information available from the μCT scans of each specimen, it was possible to account for structural variations along the length of each specimen, both in terms of the porosity and thickness. All specimens were harvested in a consistent manner with respect to location and orientation across all subjects to minimise the effects of anisotropy and inhomogeneity. Specimens of the least possible curvature were selected and it has been shown that the error caused by a small initial curvature (a mid-span curvature of $\leq 1/10^{th}$ the span length) is negligible (error <1%) (McPherson and Kriewall, 1980). The results from this study compared favourably to those in the literature and a full discussion on this comparison can be found in Motherway et. al. (2009).

The results show that impact speed plays an important role in the fracture of adult cranial bone and thus, the viscoelastic nature of cranial bone is evident. Cranial bone is naturally able to adapt with respect to its material response to protect the internal soft tissues of the cranium more effectively with increased loading rate. The morphological differences that occur between individual cranial vaults and between bone sites on a single cranium also proved important. The most notable variables are the porosity, overall bone thickness, the thickness of each of three cranial bone layers and initial radius of curvature. A large degree of variation was found to exist between cranial bones of different subjects. It was found that an increase in the percentage bone volume results in a corresponding increase in elastic modulus and the maximum bending stress. It was also found that the frontal bone tends to be thicker, less porous and have a higher percent bone volume than parietal bone and, thus, requires higher forces at fracture and absorbs more energy before fracture. Consequently, the cranial vault appears better able to resist frontal impacts as opposed to side impacts in a dynamic accident situation.

It has been possible to generate high quality FE meshes of the bone specimens and the models are currently being validated and optimised for accuracy and the reduction of computation and time costs. It is ultimately hoped to use the FE results to improve the skull material and failure definitions in the UCD 3D-FE model of the skull-brain complex, currently used to aid helmet design.

ACKNOWLEDGEMENTS

Dr. P. Verschueren, Prof. G. Van der Perre and Prof J. Vander Sloten from the Division of Biomechanics and Engineering Design, K.U. Leuven, Belgium.

REFERENCES

CAPRINO, G., IACCARINO, P., LAMBOGLIA, A. (2009). The effect of shear on the rigidity in the three-point bending of unidirectional CFRP laminates made of T800H/3900-2. Composite Structures 88, pp. 360-366.

COATS, B., MARGULIES, S. (2006). Material properties of human infant skull and suture at high rates. Journal Of Neurotrauma 23(8), pp. 1222-1232.

DELILLE, C., BAIVIER, S., MASSON, C., DRAZETIC, P. (2003). Identification des lois de comportement du crane a partir d'essais de flexion. Mechanique et Industries 4, pp. 119-123.

DELILLE, R., LESUEUR, D., POTIER, P., DRAZETIC, P., MARKIEWICZ, E. (2007). Experimental study of the bone behaviour of the human skull bone for the development of a physical head model. International Journal of Crashworthiness 12(2), pp. 101-108.

EVANS, F. G., LISSNER, H. R. (1957). Tensile and compressive strength of human parietal bone. Journal of Applied Physiology 10, pp. 493-497.

HUBBARD, R. P. (1971). Flexure of layered cranial bone. Journal of Biomechanics 4, pp. 251-263.

KANEKO, T. (1975). On Timoshenko's correction for shear in vibrating beams. Journal of Physics (D) 8, pp. 1927-1936.

MARGULIES, S. S., THIBAULT, K. L. (2000). Infant skull and suture properties: Measurements and implications for mechanisms of pediatric brain injury. Journal of Biomechanical Engineering 122, pp. 364-371.

MCELHANEY, J. H., FOGLE, J. L., MELVIN, J. W., HAYNES, R. R., ROBERTS, V. L., ALEM, N. M. (1970). Mechanical properties of cranial bone. Journal of Biomechanics 3, pp. 495-511.

MCPHERSON, G. K., KRIEWALL, T. J. (1980). The elastic modulus of fetal cranial bone: A first step towards an understanding of the biomechanics of fetal head molding. Journal of Biomechanics 13,pp. 9-16.

MOTHERWAY, J.A., VERSCHUEREN, P., VAN DER PERRE, G., VANDER SLOTEN, J., GILCHRIST, M.D. (2009). The mechanical properties of cranial bone: The effect of loading rate and cranial sampling position. Journal of Biomechanics 42, pp. 2129-2135.

PETERSON, J., DECHOW, P. C. (2002). Material properties of the inner and outer cortical tables of the human parietal bone. The Anatomical Record 268, pp. 7-15.

PETERSON, J., DECHOW, P. C., 2003. Material properties of the human cranial vault and zygoma. The Anatomical Record 274(A), pp. 785-797.

TIMOSHENKO, S., YOUNG, D. H., WEAVER (JR), W. (1975). Vibration problems in engineering. John Wiley and Sons, New York.

TIMOSHENKO, S. P., GOODIER, J. N. (1970). Theory of elasticity. McGraw-Hill Book Company, New York.

WOOD, J. L. (1971). Dynamic response of human cranial bone. Journal of Biomechanics 4, pp. 1-12.

AUTHOR LIST

1. Julie A. Motherway, Author
   Address: Rm. 217, School of Electrical, Electronic and Mechanical Engineering, University College Dublin, Belfield, Dublin 4, Ireland.
   Phone: +353 1 716 1991
   E-mail: Julie.Motherway@ucd.ie

2. Michael D. Gilchrist, Coauthor
   Address: Rm. 229, School of Electrical, Electronic and Mechanical Engineering, University College Dublin, Belfield, Dublin 4, Ireland.
   Phone: +353 1 716 1890
   E-mail: Michael.Gilchrist@ucd.ie

APPENDIX A

Finite Element Modelling- Boundary Conditions Sensitivity Analysis:

A simplified FE model of the test setup using an idealised fully homogenous bone specimen was set up to examine the effect of the model boundary conditions and also in an effort to reduce the computational cost of the model without reducing model accuracy. A number of different boundary condition set-ups were examined and the most appropriate simplification of the boundary conditions is show in Figure A1 (a). The bone material properties were average values taken from the literature (E = 9GPa, υ = 0.22). The upper impacting pin was constrained to move downwards at a fixed velocity (0.5/1/2.5 m/s). The impacting and support pins were given rigid body properties. The model was run using the Abaqus 6.9 explicit solver most suitable for dynamic situations. The elements used in the bone specimen were 8-noded linear hexahedral elements with reduced integration.

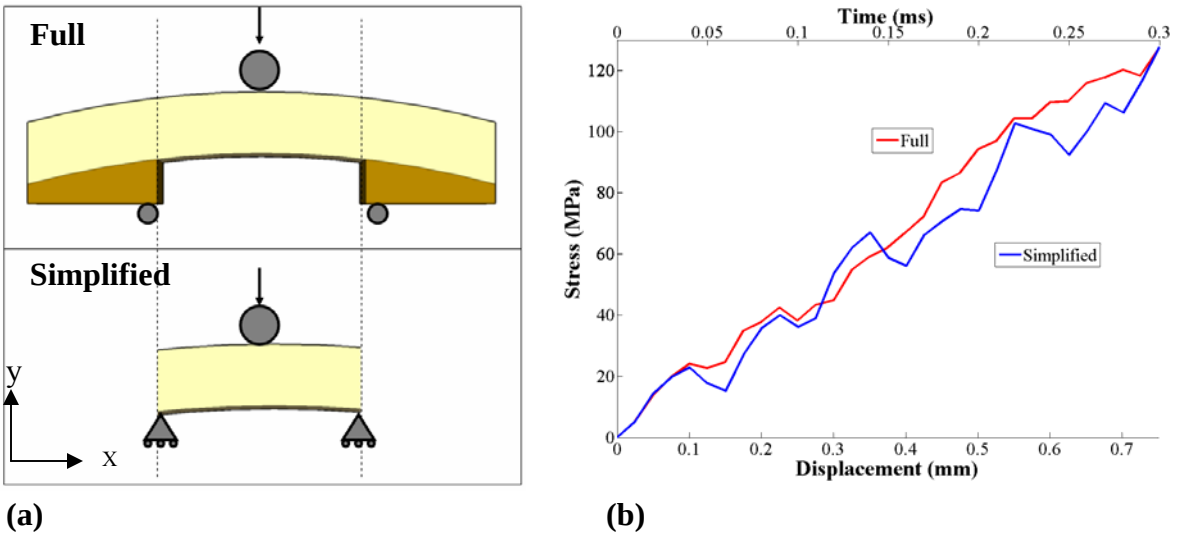

(a) **(b)**

Figure A1: (a) A schematic of the full test set-up with an idealised, fully homogeneous bone specimen (top) and the most appropriate simplified boundary conditions of the same set-up (bottom) and (b) a comparison of the tensile stress on the middle of the underneath tensile surface of the bone specimen (where fracture is expected to occur) for both the full and simplified models versus time and displacement (Test speed: 2.5m/s).

It was found that it was not necessary to model the full bone specimen but simply the central portion between the support pins and to allow the underneath edges to slide along the x plane (refer to Figure A1 (a) for orientation) but not to allow sliding in the y or z planes (z plane is into the page). Figure A1 (b) shows a comparison of the tensile stress on the underneath tensile surface of the bone specimen for both the full and simplified models. It can be seen that the simplification does not reduce the model accuracy significantly but does vastly reduce the amount of the bone specimen it is necessary to mesh and include in the analysis, thus reducing the number of nodes and elements in the model and greatly reducing the model's computation and time costs.